Superior photocatalytic activity of polypyrrole nanostructures prepared by radiolysis in water and dichloromethane

Yamina Chouli, Fatiha Belkhadem-Mokhtari, Souad Abou-Zeid, Diana Dragoe, Romuald Saint-Martin, François Brisset, Hynd Remita, Samy Remita

Superior photocatalytic activity of polypyrrole nanostructures prepared by radiolysis in water and dichloromethane

Yamina Chouli [a,b], Fatiha Belkhadem-Mokhtari [a], Souad Abou-Zeid [b], Diana Dragoe [c], Romuald Saint-Martin [c], François Brisset [c], Hynd Remita [b] and Samy Remita [b,d,*]

[a] *Laboratoire des Eco-Matériaux Fonctionnels et Nanostructurés (LEMFN), Université des Sciences et de la Technologie d'Oran- Mohamed Boudiaf, B.P. 1505 El Mnaouar, USTO, Oran, Algeria*

[b] *Institut de Chimie Physique, ICP, UMR 8000, CNRS, Université Paris-Saclay, Bâtiment 349, Campus d'Orsay, 15 Avenue Jean Perrin, 91405 Orsay Cedex, France.*

[c] *Institut de Chimie Moléculaire et des Matériaux d'Orsay, ICMMO, UMR 8182, CNRS, Université Paris-Saclay, Bâtiment 410, Campus d'Orsay, Rue du doyen Georges Poitou, 91405 Orsay Cedex, France.*

[d] *Département Chimie Vivant Santé, EPN 7, Conservatoire National des Arts et Métiers, CNAM, 292 Rue Saint-Martin, 75141, Paris Cedex 03, France*

** Corresponding author. E-mail: samy.remita@universite-paris-saclay.fr. Tel.: +33 (0)1 69 15 44 41*

Keywords: Radiolysis, Conducting polymers, Polypyrrole, Photocatalysis, Organic Photocatalysts

Abstract

Conjugated polymers have emerged as very active photocatalysts under visible light. Among these materials, nanostructured polypyrrole (PPy) has recently been used as photocatalyst for degradation of environmental pollutants under UV as well as visible light. In the present study, we specifically explored the photocatalytic activity of conducting PPy synthesized by radiolysis, either in water (PPy_{H2O}) or in dichloromethane solvent (PPy_{DCM}), in the absence of any external dopant or template. The successful preparation of both kinds of conducting polymers was confirmed by complementary spectroscopic techniques and morphological characterizations. Besides, the photocatalytic activity of both materials was evaluated in the degradation of phenol as model pollutant in aqueous solution. PPy_{H2O} as well as PPy_{DCM} were found to exhibit remarkably high photocatalytic activity under both UV and visible light. These organic photocatalysts remain very stable after several cycles and thus, easily reusable. Interestingly, PPy_{DCM} clearly appears as the most efficient photocatalyst due to its longer chain length, highly doped nature, lower optical band gap and extended absorption band from the UV to the near infrared region. The present work definitely validates radiation chemistry as an

alternative approach to synthesize conducting polymer-based photocatalysts. The obtained results also highlight that the radiosynthesized PPy, especially those prepared in dichloromethane, constitute promising candidates for photocatalytic depollution of water.

1. Introduction

Photocatalysis is one of the green and powerful chemistry that processes for reducing environmental immerging pollution in liquid and air media. However, for better employing this technology, there are many challenges to achieve such as: i) designing new materials with low energy band gap and extended photocatalytic activity under visible light (to efficiently exploit the solar energy), and ii) providing high stability to these materials for better reusability.

Solar light is composed by only 4-5% of UV. Thus, for a better use of solar light, it is important to develop photocatalytic materials which are active under visible and infra-red light. TiO_2 (Upadhyay et al., 2019) is the most commonly studied photocatalytic material. Nevertheless, the limitations in its applications result firstly from its low quantum yield due to fast charge carriers (electron/hole, e^-/h^+) recombination and secondly from its activation which occurs only under UV-irradiation because of the value of its band gap (3.2 eV for anatase and 3.0 eV for rutile) (Ohtani et al., 2010). Therefore, several strategies have been developed for modification of titania based materials in order to increase their activities under visible light, such as chemical doping (with C, N, S) (Xu et al., 2010), surface modification with metal nanoparticles (NPs) (including plasmonic metal NPs) (Kowalska et al., 2010; Mendez-Medrano et al., 2016a, 2016b; Basavarajappa et al., 2020) or coupling with other low band gap semiconducting materials (Sanchez-Rodriguez et al., 2018) to produce various kinds of titania composites (Ge et al., 2019).

Despite efforts to synthesize and improve the efficiency of such TiO_2-based photocatalytic materials, some drawbacks still remain such as complexity in synthetic methods, inhibition of oxygen radicals production and charge recombination with dopants (Liu and Chen, 2008) which weakens the separation of e^-/h^+ pairs. In this context, the use of alternative synthetic routes, especially radiolytic ones, and the development of new classes of promising photocatalysts, like conducting polymers, should be considered as robust and optimal solutions for the aforementioned limitations. In particular, such a strategy can open up the door to the efficient use of these amazing organic nanostructures for photocatalytic applications, especially for

photodegradation and mineralization of organic compounds (Floresyona et al., 2017; Ghosh et al., 2015a, 2015b).

Interestingly, conjugated polymer nanostructures recently appeared as very active under UV as well as visible light, for air and water treatment including water splitting (Ghosh et al., 2015a, 2015b, 2017; Patel et al, 2020). Also, in our recent works, their photocatalytic activity under visible light was shown to surpass even that of plasmonic TiO_2 towards pollutant removal applications. Among organic photocatalysts, polypyrrole (PPy) which is considered as one of the most promising conjugated polymers in the field of photocatalysis, can be synthesized by chemical route (Cui et al., 2014), by the way of water radiolysis (Bahry et al., 2021b; Cui et al., 2014) and by using templates such as hexagonal mesophases (Yuan et al., 2019). Note that among the latter, PPy nanostructures synthesized in hexagonal mesophases displayed interesting photocatalytic activity for water treatment under visible light and for hydrogen generation (Yuan et al., 2021, 2020). These previous studies highlighted the fact that PPy nanostructures present different photocatalytic activities depending not only on the synthetic route but also on the solvent used during synthesis. Also, the efficiency of PPy as photocatalysts was shown to depend on polymer morphology, particles size, as well as on optical and chemical states (Stejskal, 2020; Yuan et al., 2019).

In this context, we propose in the present work a facile and environmentally friendly radiolytic synthesis of polypyrrole photocatalysts in both aqueous solution (PPy_{H2O}) and organic solvent, namely dichloromethane (PPy_{DCM}). The first aim is to easily prepare efficient and reusable photocatalysts without using any external dopant and any template and second to compare the photocatalytic activity of radiosynthesized PPy materials with those of conjugated polymer based photocatalysts already described in literature. A particular emphasis will be put on PPy_{DCM} synthesized by radiolysis in dichloromethane which is shown in the present work to be not only a very good and efficient candidate for photocatalytic degradation of organic pollutants, such as phenol, but also very stable with cycling.

2. Experimental

2.1. Reagents, atmospheres and solvents

Pyrrole, Py, (98% purity) was used as monomer for polypyrrole (PPy) synthesis. Dichloromethane (DCM) anhydrous (≥ 99.8%, purchased from Sigma-Aldrich) and distilled water (Millipore system 18.2 MΩ cm) were used as solvents. Nitrous oxide (N_2O) and Nitrogen

(N_2) (from Air Liquid Co. with purity 99.99 %) were respectively used for degassing aqueous or dichloromethane solutions before γ-irradiations. Phenol (≥ 99.5% purity) was used as an organic model pollutant. Acetonitrile (ACN) (≥ 99.9%, purchased from Sigma-Aldrich) was used for HPLC measurements. All reagents were used as received without any further treatment or purification. All experiments were performed at room temperature.

2.2. Preparation of polymer-based photocatalysts

For the preparation of our organic PPy-based photocatalysts, we followed the radiation-based methodology developed in our previous studies (Cui et al., 2014; Bahry et al., 2021b) with some modifications in terms of Py monomer concentrations and irradiation doses. In the present work, two Py monomer solutions were prepared with two different solvents, water and dichloromethane, under two different atmospheres (**Scheme 1**). In the first solution, Py monomers were dissolved in water at a concentration of 20 mM. The solution was then degassed for 20 minutes under N_2O. In the second solution, Py monomers, also at a concentration of 20 mM, were dissolved in DCM and the solution was then degassed for 20 minutes under N_2.

Both prepared solutions were then placed under γ-irradiation at an irradiation dose of 72 kGy at a dose rate of about 4 $kGy.h^{-1}$. The irradiations were performed with a ^{60}Co panoramic γ-ray source. The irradiation dose chosen for both solutions is totally justified and reasoned. Indeed, as explained in our previous works, water radiolysis under N_2O leads to the generation of hydroxyl radicals ($HO^{\cdot}$) which efficiently oxidize Py monomers leading to their polymerization (Cui et al., 2014; Bahry et al., 2021b). In particular, it was shown that an irradiation dose of 72 kGy is required for the quantitative polymerization in water of Py (20 mM) into PPy polymers (PPy_{H2O}), according to **Scheme 1**. On another hand, we also demonstrated that chloromethyl ($CH_2Cl^{\cdot}$) and dichloromethyl ($CHCl_2^{\cdot}$) radicals, produced during DCM radiolysis under N_2, also quantitatively oxidize Py monomers (Bahry et al., 2020, 2021a, 2021b). Based on our work (Bahry et al., 2021b), the dose needed for the quantitative polymerization in DCM of Py (20 mM) into PPy polymers (PPy_{DCM}) is once again 72 kGy, according to **Scheme 1**.

Irradiation at 72 kGy of both samples (Py in water or in DCM) led to two black, aqueous and organic, suspensions. The irradiated solution of PPy_{H2O} was centrifuged at 8000 rpm for 30 minutes. A black PPy_{H2O} precipitate was then obtained. Differently, after irradiation, DCM solvent was removed from the suspension of PPy_{DCM} by using a rotary evaporator. A black PPy_{DCM} precipitate was then obtained. PPy_{H2O} and PPy_{DCM} polymer deposits were then dried at

60°C for 24h to get the final black solid powders. Afterwards, these two solid samples were characterized by complementary techniques and finally used as photocatalysts.

2.3. Characterization of polymer materials

UV-Vis absorption spectroscopy. This technique was used to check the optical properties in solution of Py monomers before irradiation and those of PPy_{H2O} and PPy_{DCM} polymers radiosynthesized in water and DCM at 72 kGy, respectively under N_2O and N_2 atmospheres. A HP 8543 spectrophotometer was used to measure the absorbance of all solutions.

Attenuated Total Reflectance Fourier Transform Infrared (ATR-FTIR) spectroscopy. ATR-FTIR spectroscopy was used for chemical characterization of radiosynthesized PPy_{H2O} and PPy_{DCM} polymers. The dried polymers were deposited and squeezed on the ATR support of the FTIR spectrophotometer. Measurements were recorded by using a Bruker Vertex 70 FTIR spectrophotometer and infrared spectra were recorded between 600 and 4000 cm^{-1}.

X-ray Photoelectron Spectroscopy (XPS). XPS spectroscopy was used to identify the chemical states of dried PPy_{H2O} and PPy_{DCM} polymer powders. XPS analysis was conducted under argon atmosphere on a Thermofisher Scientific K-Alpha instrument equipped with an Al Kα monochromatic X-Ray source (Al-Kα, hν = 1486.7 eV). A spot of 400 μm with a hemispherical analyzer, operating at a pass energy of 200 eV and a step of 1 eV, was used for recording the general survey spectra. Differently, for the narrow scans, a pass energy of 50 eV and a step of 0.1 eV were used. Thermo Scientific™ Avantage software was used for treating and interpreting data acquisition.

X-Ray Diffraction (XRD) analysis. XRD analysis was used to check the crystallinity of radiosynthesized PPy_{H2O} and PPy_{DCM} polymers which were first crushed and hand-milled in order to obtain fine powders. XRD characterization was conducted on an X-ray diffractometer PANalytical X'pert pro MPD with X'celerator acquisition system. The Cu Kα1 radiation (λ = 1.54059 Å) radiation was used as the X-ray source. The intensity detected was recorded as a function of the angle of deflection 2θ of the beam from 10° to 80°.

Scanning Electron Microscopy (SEM). SEM microscopy was used to investigate the structure of radiosynthesized PPy_{H2O} and PPy_{DCM} polymers. The dried polymers were deposited onto carbon tape adhered to aluminum mounts. The SEM observations were performed by using a ZEISS Supra 55-VP FEG-SEM microscope operating at 1 kV.

Transmission Electron Microscopy (TEM). TEM microscopy was used to investigate the structure, size and morphology of radiosynthesized PPy_{H2O} and PPy_{DCM} polymers. Few drops of each irradiated solution were first dispersed in ethanol, then deposited onto carbon-coated copper grids and dried under N_2 flow. A JEOL JEM-2010 microscope operating at an accelerating voltage of 200 kV was used. The micrographs were collected by using a Gatan Rio CMOS 16 camera.

2.4. Evaluation of photocatalytic activity of polymer materials

The photocatalytic activity of radiosynthesized PPy_{H2O} and PPy_{DCM} polymers was evaluated for the photodecomposition of phenol (C_6H_5OH, chosen as a model pollutant) in water. Indeed, it is well known that phenolic compounds are real contaminants of water with very high toxicity. Besides, the choice of phenol as model pollutant was guided by different favourable characteristics: i) phenol is not photosensitive, ii) its degradation mechanism and products are well known and already identified by using High Performance Liquid Chromatography (Andrade et al., 2006; Cristina Sertori Paschoalino et al., 2012; Mesa et al., 2020) and iii) it can be completely mineralized into CO_2 and H_2O.

At first, an aqueous solution containing phenol pollutant (50 ppm) was prepared. 3 mg of dried PPy_{H2O} powder were added to 3 mL of this phenol solution in a quartz cell reactor while 3 mg of dried PPy_{DCM} powder were added to 3 mL of the same solution in another quartz cuvette. The two obtained suspensions were stirred carefully in the dark in order to attain the adsorption-desorption equilibrium before irradiation.

Before any photocatalytic test, dark adsorption tests of PPy_{H2O} and PPy_{DCM} polymers were carried out in the presence of phenol but in the absence of UV or Visible light irradiation in order to check the adsorption of the model pollutant onto the surfaces of the photocatalysts.

The degradation of phenol in presence of radiosynthesized PPy_{H2O} and PPy_{DCM} polymers was then studied under UV and visible light irradiations. The two obtained suspensions were irradiated in the quartz cuvettes with an Oriel 300 W xenon lamp under bubbling with O_2 at a fixed flow rate, along with continuous magnetic stirring. For experiments under visible light irradiation, an ultraviolet optical cut-off filter ($\lambda > 400$ nm) was specifically used.

Every 10 minutes (under UV-Vis light irradiation) and every 1 hour (under Visible light irradiation), 400 µL of each suspension were collected, and centrifuged for 30 minutes at 13 000 rpm. The resulted supernatants were systematically analyzed by High Performance Liquid Chromatography (HPLC) in order to determine the effective concentration of phenol

and to evaluate its degradation. HPLC apparatus was supplied by Agilent Technologies (HPLC, Agilent 1260 Infinity Quaternary LC) and used with a mobile phase of 80 vol% H_2O and 20 vol% acetonitrile. In order to follow the photodegradation of phenol, the ratio C/C_0 was studied as a function of irradiation time. Note that C_0 is the initial concentration of phenol and C is the concentration of phenol after sampling in regular time intervals. Multiple photocatalysis experiments were performed under identical reaction conditions to verify the reproducibility of the measurements.

After completion of the degradation of phenol, both PPy_{H2O} and PPy_{DCM} polymer photocatalysts were recovered by filtration, washed many times with distilled water and dried at 60°C overnight. In order to check their stability upon cycling, these already-used photocatalysts were then re-employed in another cycle to check their efficiency in the photocatalytic degradation of phenol under identical experimental conditions. These steps were repeated up to 4 cycling experiments. The photodegradation rate of phenol for each cycle was finally evaluated by using the following formula:

$$\text{Degradation rate (\%)} = \frac{C0-C}{C0} \times 100 \qquad \textbf{(1)}$$

3. Results and Discussion

3.1. Radiation induced synthesis of PPy_{H20} and PPy_{DCM}

Aqueous and dichloromethane solutions containing 20 mM Py monomers both appear colorless before irradiation (inset of **Figure 1a**). Their absorption spectra display the characteristic peak of Py monomers at 205 nm (inset of **Figure 1a**), usually ascribed to π-π* transitions in pyrrole, in good agreement with literature (Bahry et al., 2021b).

According to our previous studies, starting from 20 mM in Py monomers, the complete and optimal PPy synthesis either in water under N_2O or in DCM under N_2 atmosphere is always attained at 72 kGy. The UV-Vis absorption spectra of PPy_{H2O} and PPy_{DCM} polymers produced in these conditions are displayed in **Figure 1a**. Note that the two solutions, which were colorless before irradiation, transformed to black suspensions as exhibited in **Figure 1a**. The change in UV-Vis absorption spectra and in colors of both solutions upon irradiation are indicative of the successful synthesis of polymer materials both in water and DCM. Moreover, the quantitative production of PPy polymers upon radiolysis is confirmed by the quasi-disappearance of the characteristic peak of Py monomers positioned at 205 nm within the spectra of irradiated solutions.

The UV-Vis absorption spectrum of PPy_{H2O} is in good agreement with previous studies (Cui et al., 2014; Bahry et al., 2021b). It displays a shoulder in the range of 350–400 nm which is attributed to the formation of PPy oligomers and which can be ascribed to the π−π* transitions along the oligomer chains (**Figure 1a**). In addition, a continuous scattering (long absorption tail) is observed in the extinction spectrum of PPy_{H2O}, in the range 400−1000 nm, which should result from the presence of the black suspension present in the sample. Note that this suspension remains relatively stable and that no sedimentation process occurs over a few days after irradiation. This could be explained by the relatively low molecular weight of PPy_{H2O} oligomers as well as by their hydrophilicity.

The UV-Vis absorption spectrum of PPy_{DCM} is different from that of PPy_{H2O} (**Figure 1a**). By comparing the two spectra, one can note that spectral features of PPy_{DCM} are clearly more prominent than those observed in case of PPy_{H2O}. In addition to the absorption band observed at around 350 nm, ascribed to the π−π* transitions, PPy_{DCM} spectrum displays a shoulder at 530 nm together with a broad band at higher wavelengths in the range 700-1100 nm with a maximum absorption at 930 nm. When comparing with PPy_{H2O}, PPy_{DCM} spectrum is red-shifted which is attributed to the formation of PPy_{DCM} polymers possessing higher molecular weight. Note that we unsuccessfully attempted to estimate and compare the molecular weights and the polymer chain lengths of PPy_{H2O} and PPy_{DCM} by size-exclusion chromatography (SEC). Indeed, the solubility of both radiosynthesized polymers was too low in the different solvents usually used in SEC chromatography (such as acetone, acetonitrile and THF). Besides, when comparing with PPy_{H2O} spectrum, the large absorption band at 930 nm observed in PPy_{DCM} spectrum corresponds to polaron and bi-polaron bands, originating from the oxidized state of doped PPy_{DCM} polymers in agreement with previous works (Cui et al., 2014; Bahry et al., 2021b, 2020; Chen et al., 2015; Li et al., 2010). Indeed, as highlighted in literature and contrarily to water radiolysis which leads to non-doped PPy materials, dichloromethane radiolysis generates chloride ions which enable *in situ* production of doped PPy polymers (Cui et al., 2014; Bahry et al., 2021b, 2020, 2018).

In order to calculate and compare the optical band gaps (Eg) of radiosynthesized PPy_{DCM} and PPy_{H2O}, Tauc plots were used (Tauc and Menth, 1972). These plots (**Figure 1b** and **Figure 1c**) can be easily read out from the UV-Vis absorption spectra of both PPy_{H2O} in aqueous solution and PPy_{DCM} in DCM solvent (**Figure 1a**). In the context of Tauc plots, based on Tauc equation applied to amorphous materials (such as radiosynthesized PPy as it will demonstrated

in **section 3.3**), $(\alpha h\nu)^{1/2}$ must be plotted as a function of photon energy ($h\nu$) (Ghobadi, 2013) according to:

$$(\alpha h\nu)^{1/2} = A(h\nu - Eg) \quad \textbf{(2)}$$

where α, h, ν and Eg are respectively the absorption coefficient, Planck constant, light frequency and optical band gap energy and where A is a constant.

The Tauc plots of PPy_{H2O} and PPy_{DCM} are respectively displayed in **Figure 1b** and **Figure 1c**. Besides, plotting $(\alpha h\nu)^{1/2}$ as a function of photon energy ($h\nu$) enables the determination of the two optical band gaps (Eg) by extrapolating the straight-line portion of the Tauc plots to the photon energy axis. While the optical band gap of PPy_{H2O} amounts to 2.31 eV, that of PPy_{DCM} is about 1.30 eV.

These two optical band gaps values characterizing PPy_{H2O} and PPy_{DCM} are in good agreement with our previous works on radiation induced conducting polymers (Bahry et al., 2021b) as they remain relatively low. Nevertheless, the band gap value of PPy_{DCM} is much lower than that of PPy_{H2O}. This interesting result can be easily explained by the longer polymer chains and by the doping state of PPy_{DCM} polymers synthesized by using radiolysis dichloromethane solvent (Abdulla and Abbo, 2012).

Interestingly, the low band gap value of PPy_{DCM} materials together with their intense absorption in the UV and Visible domains are triggering hopes for a higher photocatalytic activity in the whole solar spectrum. This will be discussed at a later stage of the work.

3.2. Chemical characterization of PPy_{H20} and PPy_{DCM}

In order to investigate and compare the chemical compositions of the as-synthesized PPy_{H2O} and PPy_{DCM} polymers, ATR-FTIR analysis was performed on the black PPy powders obtained after solvent removal (photographs within **Figure 2**). The infrared spectra of PPy_{H2O} and PPy_{DCM} were recorded within a wavenumber region from 600 to 4000 cm^{-1} as displayed in **Figure 2**.

The FTIR spectra of PPy obtained in both solvents by water and DCM radiolysis are in very good agreement with the literature (Kato et al., 1991; Vetter et al., 2011; Rezaul Karim et al., 2007; Cui et al., 2014; Bahry et al., 2021b) where all the infrared peaks observed in the present work were already described and ascribed, highlighting the successful radiation-induced synthesis of PPy materials.

Also, aside from a difference in the intensity and the shape of the bands around 3200 cm^{-1} and the presence of an additional peak at 1677 cm^{-1} in PPy_{DCM} spectrum, no significant

differences exist between PPy_{H2O} and PPy_{DCM} spectra. Only small shifts in the vibration modes can effectively be observed. For instance, PPy_{H2O} spectrum shows =C–H out-of-plane vibration band at 793 cm^{-1} (792 cm^{-1} in case of PPy_{DCM}) and =C–H in-plane, and C-C out-of-plane vibration between 1047 cm^{-1} and 1262 cm^{-1} (between 1051 cm^{-1} and 1263 cm^{-1} in case of PPy_{DCM}) (Karim et al., 2007; Kato et al., 1991; Vetter et al., 2011; Bahry et al., 2021b; Cui et al., 2014). Besides, the weakest bands at around 1346 cm^{-1} (for both polymers) and 1411 cm^{-1} for PPy_{H2O} (1421 cm^{-1} for PPy_{DCM}) can be attributed to the C–N stretching vibration in the pyrrole rings (Rezaul Karim et al., 2007; Bahry et al., 2021b). Also, the peak at 1535 cm^{-1}, which appears as a shoulder in PPy_{H2O} spectrum corresponds to the C=C and C–C stretching vibrations of pyrrole rings within polypyrrole polymers (Karim et al., 2007; Kato et al., 1991).

When focusing on the differences between the two infrared spectra, one can notice the surprising presence in PPy_{H2O} spectrum of an intense peak at 1677 cm^{-1}. Nevertheless, such a band has already been observed in literature specifically when polymerizing Py monomers in water. This peak was attributed to the presence of C=O carbonyl groups which highlights the overoxidation state of polypyrrole when quantitatively synthesized in water (Mathys and Truong, 1997; Cui et al., 2014; Vetter et al., 2011). One can then conclude that at 72 kGy (dose required for complete polymerization of both materials), contrary to PPy polymers which are found overoxidized when synthesized in aqueous medium, the use of DCM solvent for radiation induced Py polymerization clearly avoids PPy overoxidation.

Now, when considering the two spectra in the domain of highest wavenumbers, the large bands observed at 3282 cm^{-1} in case of PPy_{H2O} and at 3144 cm^{-1} in case of PPy_{DCM} are both attributed to the in-plane stretching of N–H groups in PPy polymers (Gürbüz et al., 2017; Kato et al., 1991; Lei and Martin, 1992). The broadness of these bands can be explained by the hydrogen bond interactions which exist between the N-H groups present all along the polymer chains. The more intense band observed in case of PPy_{H2O} should result from the specific presence within these polymers of carbonyl groups which evidently favor such hydrogen bond interactions.

As highlighted in previous works, FTIR spectra of Py monomers before irradiation display a band at 734 cm^{-1} either in water or in DCM (Cui et al., 2014; Bahry et al., 2021b), which is characteristic of C−H wag vibration at α, α′ positions (see **Scheme** 1, results not shown). However, interestingly, one can note the absence of such a band in both PPy_{H2O} and PPy_{DCM} FTIR spectra. This finding proves the total consumption of Py monomers and confirms the successful and quantitative radiolytic production of PPy polymers, through α-α' coupling reactions according to **Scheme 1**, either in water or in DCM solvent.

As a complement to ATR-FTIR study, XPS analysis was performed in order to get further insight concerning the surface elemental composition and chemical states of both PPy_{DCM} and PPy_{H2O} samples. The wide scans (General Survey spectra) as well as the C1s and N1s core-levels spectra obtained for the two polymer samples are presented in **Figure 3**.

The two survey spectra of **Figure 3** show the presence of carbon, nitrogen, and oxygen atoms (peaks with variable intensities) as already observed in literature in the case of PPy polymers synthesized by conventional methods (Šetka et al., 2019; Tabačiarová et al., 2015). Given the formula of the polymer (see **Scheme 1**), the presence of carbon and nitrogen in both samples is totally comprehensible. The presence of oxygen in PPy_{H2O} is also logical and can easily be explained by the presence of C=O functionalities within overoxidized polymers as highlighted by ATR-FTIR spectroscopy. In PPy_{DCM} sample, the amount of oxygen is far lower since no overoxidation happens in DCM solvent. Nevertheless, the presence of oxygen, even in trace amounts, within PPy_{DCM} sample was not expected. The unexpected presence in trace amounts of oxygen in this case could be due to a chemical contamination by small amounts of water since DCM solvent that was employed during radiolysis was used without prior distillation.

Interestingly, in case of PPy_{DCM}, one can observe in the spectrum (**Figure 3**) the specific presence of an additional peak located at 200.8 eV. Such a peak is undoubtedly attributable to chlorine atoms which are present in PPy_{DCM} polymers, but not in PPy_{H2O}. Interestingly, in previous works concerning chemical synthesis of polypyrrole materials, such a $Cl2p_{3/2}$ peak was observed and assigned to Cl atoms linked to PPy carbon chains (Feng et al., 2020; Tabačiarová et al., 2015). In our case, this observation is in good agreement with DCM radiolysis which produces reactive chloromethyl ($CH_2Cl^{\cdot}$) and dichloromethyl ($CHCl_2^{\cdot}$) radicals (that can add to PPy carbon chains) and which also generates HCl and Cl^- (that can dope PPy polymers) (Bahry et al., 2021b, 2020, 2018). This definitely demonstrates that PPy_{DCM} synthesized by radiolysis in DCM are *in situ* doped with chlorine atoms, in total agreement with our results obtained by UV-vis absorption spectroscopy.

Let's now consider the individual C1s core-level spectra of PPy_{H2O} and PPy_{DCM} conducting polymers (**Figure 3a and 3c**). Both spectra were fitted using the same components. The characteristic peaks at 284.3 eV, 284.9 eV, 285.7 eV, 286.7 eV and 288.3 eV are attributed, in agreement with literature, to β carbon, α carbon, C–N, C–O and C=O respectively (Feng et al., 2020; Šetka et al., 2019). As already observed and mentioned, the contribution of oxygen is noticeably larger in PPy_{H2O} sample due to overoxidation. Interestingly, PPy_{DCM} carbon level

spectrum specifically exhibits an additional peak at 287.7 eV, which was attributed in literature to $–C=N^+$ of bipolaron charge species in polypyrrole (Feng et al., 2020; Šetka et al., 2019).

When considering the individual N1s core-level spectra of PPy_{H2O} and PPy_{DCM} materials (**Figure 3b and 3d**) which highlight similarities, the binding energies of 398.3 eV, 399.7 eV and 400,3 eV respectively correspond to the =N– imine like nitrogen (Setka et al., 2020; Šetka et al., 2019; Tabačiarová et al., 2015), to the –N–H– structures (Ge et al., 1994; Malitesta et al., 1995; Pfluger and Street, 1984) and to the $–N–H^+–$ polaron within PPy polymers. At higher binding energy and specifically in case of PPy_{DCM}, one can observe the presence at 401.9 eV of an additional peak which was ascribed in literature to the $=N–H^+–$ bipolaron charge species within polypyrrole (Malitesta et al., 1995; Pfluger and Street, 1984; Šetka et al., 2019).

In agreement with ATR-FTIR spectroscopy and UV-Vis absorption spectrophotometry, XPS analysis demonstrates that PPy_{H2O} polymers are found overoxidized when produced by water radiolysis at 72 kGy, while PPy_{DCM} materials are *in sit*u doped and thus produced in an oxidized state during DCM radiolysis at the same irradiation dose. The doping state of PPy_{DCM} explains in particular its relatively low band gap value as found by Tauc plot (**Figure 1c**).

3.3. Structural and morphological characterizations of PPy_{H20} and PPy_{DCM}

In order to investigate the crystallinity of PPy_{H2O} and PPy_{DCM} polymers produced by water and DCM radiolysis, X-ray diffraction (XRD) analysis was performed on the black PPy powders obtained after solvent removal (**Figure 4**). The typical X-ray diffraction patterns characterizing the two polymers are exhibited in **Figure 4**. The two diffractograms look somewhat similar, highlighting the fact that PPy_{H2O} and PPy_{DCM} have the same structure.

Both XRD patterns display a broad diffraction peak at about $2\theta \sim 20°$, meaning, in agreement with literature (Chougule et al., 2012, 2011), that both radiosynthesized PPy_{H2O} and PPy_{DCM} materials have an amorphous structure (Warren and Madden, 2006), this structural disorder being due to the scattering of PPy carbon chains at the interplanar spacing (Wynne and Street, 1985). Note that the amorphous structure of both PPy polymers justifies and legitimizes the use of equation (2) in **section 3.1** in the context of Tauc plots.

In order to investigate the morphology and the size of PPy_{H2O} and PPy_{DCM} materials produced by radiolysis, SEM and TEM observations were performed. Typical SEM images recorded after deposition of dried PPy_{H2O} and PPy_{DCM} polymer powders are displayed on **Figure 5a and 5b** respectively. **Figure 5a (**characterizing PPy_{H2O} sample) highlights the

presence of aggregated spheroidal particles. The same observations were made throughout the whole sample. These packed globular PPy_{H2O} particles which are heterogeneous in size (between 200 nm and 800 nm) have a mean diameter of few hundreds nm. Besides, **Figure 5b (**characterizing this time PPy_{DCM} sample) also displays spheroidal particles (heterogeneous in size, between 200 nm and 1.5 μm) with relatively larger average size. Same observations were once again made in the whole PPy_{DCM} sample. Note that the observation of such aggregated spheroidal particles in the case of radiosynthesized conducting polymers is in very good agreement with literature (Cui et al., 2014; Bahry et al., 2018, 2020). Each observed PPy_{H2O} or PPy_{DCM} particle should be composed of linear chain polymers which are neither branched nor networked but in weak interactions (by hydrogen bonds or π-stacking interactions).

As a complement to SEM microscopy, TEM observations were performed in order to get further insight concerning the morphology of both PPy_{H2O} and PPy_{DCM} samples. This time, few drops of each irradiated solution were deposited onto carbon-coated copper grids then dried under N_2 flow. Representative TEM images obtained in case of PPy_{H2O} and PPy_{DCM} polymers are displayed on **Figure 5c and 5d** respectively. Low-density globular structures forming polydisperse spherical nanoparticles are observed in both cases. PPy_{H2O} polymers have a mean diameter of few hundreds nm (**Figure 5c**), while bigger PPy_{DCM} polymer particles, up to 1.5 μm in size, are observed (**Figure 5d**) in very good agreement with SEM observations. Also, in all our TEM observations, PPy_{H2O} and PPy_{DCM} particles systematically appear self-assembled into supramolecular nanochaplets (thanks to interparticle interactions). This result is in good agreement with a previous observation, made by cryo-TEM microscopy, of PPy synthesized in water by radiolysis (Cui et al., 2014).

The observations made by SEM and TEM microscopies in the present work as well as the characterizations conducted by XRD analysis enable us to conclude without any ambiguity that radiolysis of Py monomers in both water and DCM solvents leads to the production of amorphous PPy polymers, made of polydisperse spherical nanoparticles. Clearly, the nature of the solvent (water or DCM) used during radiolysis does not impact the morphology nor the crystallinity of radiosynthesized polymers. Interestingly, even if PPy_{DCM} nanoparticles appear always slightly larger than PPy_{H2O} ones, the similarity between the results obtained by SEM and TEM indicates that the drying process as well as the deposition procedure do not affect the size and the shape of the particles. This highlights the stability of our radiosynthesized materials

as well as the existence of relatively strong interactions (π-stacking and hydrogen-bond interactions) into each polymer particle whatever the solvent used during radiolysis.

3.4. Photocatalytic activity assessment of PPy_{H20} and PPy_{DCM}

Two kinds of polymers, namely PPy_{H2O} and PPy_{DCM}, were first prepared by radiolysis and then chemically, structurally and morphologically characterized by complementary techniques. The photocatalytic activity of both radiosynthesized polymers was finally investigated for the photodecomposition in water of phenol (C_6H_5OH), which was chosen as a model pollutant.

To this end, two aqueous solutions (3 mL) each containing 50 ppm of phenol pollutant were prepared in the dark: the first one in presence of 3 mg of dried PPy_{H2O} powder and the second one in presence of the same amount of dried PPy_{DCM} powder. Before any irradiation and any photocatalytic experiment, dark adsorption tests were carried out on both samples in order to check the adsorption of the model pollutant onto the surfaces of PPy_{H2O} and PPy_{DCM} polymers. Interestingly, as highlighted by HPLC (results not shown), no decrease in the concentration of phenol was observed even after few hours, highlighting the fact that this model pollutant does not adsorb onto the surfaces of the photocatalysts and that any further decrease in phenol concentration under irradiation should only be attributed to a photocatalytic degradation (and not to an eventual adsorption).

After these preliminary dark adsorption tests, both samples were subjected to UV and visible light irradiations under O_2 flow. The degradation of phenol in presence of PPy_{H2O} or PPy_{DCM} polymers, now employed as photocatalysts, was then assessed by using HPLC. In both cases, the ratio C/C_0 (as deduced from HPLC) was studied as a function of irradiation time either under UV-light irradiation (**Figure 6a**) or under visible-light irradiation (**Figure 6b**).

When considering UV-irradiation, the decay in phenol concentration is clearly observed as a function of irradiation time in both PPy_{H2O} and PPy_{DCM} cases (**Figure 6a**), highlighting the fact that both materials act as photocatalysts under UV. Nevertheless, from the comparison between the two curves of **Figure 6a**, one can note that the degradation of phenol under UV is much faster in the presence of PPy_{DCM}. In particular, while the total consumption (100 %) of phenol is reached after 80 minutes in the case of PPy_{DCM}, only 50 % of phenol is consumed in the presence of PPy_{H2O} even after 120 minutes. Clearly, the photocatalytic activity of PPy_{DCM} for phenol degradation is much higher than that of PPy_{H2O} under UV light.

Also, the degradation of phenol in presence of PPy_{DCM} was followed by HPLC as a function of UV-irradiation time (results not shown). In agreement with literature (Andrade et al., 2006;

Cristina Sertori Paschoalino et al., 2012; Mesa et al., 2020), HPLC results clearly showed that first degradation step (at intermediate irradiation times) consists in oxidation of phenol into phenol intermediates (catechol, hydroquinone, and benzoquinone). Interestingly, after 80 minutes UV-irradiation, HPLC analysis clearly highlighted the total disappearance of both phenol and its intermediates, indicating the quantitative degradation and mineralization in these conditions of the model pollutant.

PPy_{DCM} appears as a very efficient photocatalyst under UV for the degradation of organic pollutants. But what about its activity and that of PPy_{H2O} under visible light irradiation? Indeed, an important challenge in photocatalysis is to develop photocatalytic materials which are active in the visible light region. In order to answer this question, the photocatalytic activity of PPy_{DCM} and PPy_{H2O} materials was then studied in this spectral region. As in the case of UV-irradiation, the decay in phenol concentration under visible light irradiation is clearly observed as a function of irradiation time in both PPy_{H2O} and PPy_{DCM} cases (**Figure 6b**), highlighting the fact that both materials also act as photocatalysts in the visible light region. Nevertheless, one can note that phenol degradation is less efficient than under UV, particularly in the case of PPy_{H2O} material.

As observed in the case of UV-irradiation, from the comparison between the two curves of **Figure 6b** obtained under visible light irradiation, one can note that the degradation of phenol is much faster in the presence of PPy_{DCM}. In particular, PPy_{DCM} photocatalyst shows a relatively high degradation rate of 50% after 300 minutes, whereas only 12% degradation is reached after the same irradiation time with PPy_{H2O} as photocatalyst. Clearly, the photocatalytic activity of PPy_{DCM} for phenol degradation under visible light is much higher than that of PPy_{H2O}, as in the case of UV light irradiation.

Many factors can impact the photocatalytic activity of a material, such as size, morphology, electrical state and hole/electron recombination rate (Ghosh et al., 2015b, 2015a). In particular, we have already shown that the nanostructuration of a conjugated polymer-based photocatalyst is a key factor which determines the photocatalytic efficiency of the material. Higher surface area and lesser number of defects in nanostructured polymers (which induce less electron-hole recombinations), lead to higher photocatalytic activity. Nevertheless, as demonstrated in the present work, both radiosynthesized PPy_{H2O} and PPy_{DCM} appear as nanostructured materials with comparable morphologies. As a consequence, the superior photocatalytic activity of PPy_{DCM} which is observed here, in the whole solar spectrum, comes essentially from its doping state that positively impacts its optical band gap energy (Eg =1.30 eV), which is much lower than that of PPy_{H2O} (Eg = 2.31 eV), and from its absorption in the visible-near IR region, which

is much larger than that of PPy_{H2O}, as earlier highlighted by UV-Vis absorption spectra and by the corresponding Tauc plots (**Figure 1**).

Let's now compare the photocatalytic efficiency of PPy_{DCM} materials, synthesized in the present work by DCM radiolysis, with activities of other kinds of materials previously used in literature for photocatalytic degradation of phenol as model pollutant. Let's also limit the comparison and the discussion to the most efficient conducting polymer based photocatalysts which have anteriorly been described in literature (Ghosh et al., 2015a, 2015b; Floresyona et al., 2017; Yuan et al., 2019).

Among the most interesting results available in literature, the best photocatalytic activity was obtained by using PEDOT nanospindles which were chemically synthesized within hexagonal mesophases as soft templates (Ghosh et al., 2015b). Indeed, the total consumption (100 %) of phenol was reached after only 10 minutes under UV light and after 240 minutes under visible light. This extraordinary efficiency was explained by the nanostructuration of PEDOT nanospindles within mesophases during chemical synthesis and by their relatively low electrochemical band gap (1.69 eV) together with their extended visible light absorption ability.

The same synthetic approach, based on the use of soft templates, was then pursued in order to prepare new efficient conducting polymer based photocatalysts: PDPB nanofibers (Ghosh et al., 2015a) were successfully synthesized by photopolymerization within hexagonal mesophases, while PPy (Yuan et al., 2019) and P3HT (Floresyona et al., 2017) nanostructures were obtained by chemical polymerization in the same hexagonal self-assemblies. Nevertheless, the results obtained in the latter cases for phenol degradation were less interesting than those obtained with PEDOT nanospindles. Indeed, on the first hand, PDPB photocatalysts showed a degradation rate of 82 % under UV light after 270 minutes and of 70 % under visible light after the same time (Ghosh et al., 2015a). Also, on the second hand, PPy nanostructures chemically prepared within hexagonal mesophases were characterized by slightly higher activity under UV but much lower activity under visible light: a degradation rate of 100 % under UV light was reached after 270 minutes, while only 10 % degradation was reached after 300 minutes under visible light (Yuan et al., 2019). Finally, P3HT nanostructures chemically synthesized within soft templates were characterized by a degradation rate of 90 % under UV light after 180 minutes and of 16 % under visible light after 240 minutes (Floresyona et al., 2017). When comparing conducting polymer nanostructures prepared in hexagonal mesophases, the much lower photocatalytic activity of PDPB, PPy and P3HT nanostructures (in comparison with that of PEDOT nanospindles) was explained by their relatively high optical

and electrochemical band gap values (Ghosh et al., 2015a, 2015b; Floresyona et al., 2017; Yuan et al., 2019).

In the present work, instead of chemical or photochemical polymerizations, we used an alternative radiolytic route for synthesizing conducting polymer based photocatalysts. And notably, we prepared photocatalytic materials in the bulk of water or DCM solvent in the absence of any chemical template. Interestingly, despite the simplicity of our methodology, we obtained PPy_{DCM} materials with very encouraging photocatalytic properties thanks to their very low optical band gap and their large extended absorption band. Indeed, under UV light (degradation rate of 100 % after 80 minutes), the activity of PPy_{DCM} is much higher than that of PDPB, PPy and P3HT nanostructures prepared in hexagonal mesophases. Only PEDOT nanospindles, also prepared in soft templates, appear more efficient under UV since the time needed for complete degradation of phenol is shorter (10 minutes instead of 80). Also, under visible light (degradation rate of 50 % after 300 minutes for radiosynthesized PPy_{DCM}), even if the photocatalytic activity of PPy_{DCM} remains two times lower than that of PEDOT nanospindles, it is still higher than that of PPy and P3HT nanostructures prepared in hexagonal mesophases and appears almost comparable with that of PDPB nanofibers.

The stability over time and upon cycling of photocatalytic materials is a key factor for their effective use in industrial and environmental applications. In order to check the stability upon cycling of PPy_{DCM}, this material was re-employed up to 4 cycling experiments under identical conditions in the context of phenol photodegradation under UV irradiation. The photodegradation rate of phenol for each cycle was evaluated by using **equation (1)** and the obtained results are displayed in **Figure 6c**.

As already described in case of PPy_{DCM}, in the first photocatalytic cycle, the total consumption (100 %) of phenol is reached after 80 minutes. As observed in **Figure 6c**, during the following cycles, after the same time, the photodegradation rate remains almost close to 100 % and slightly decreases, reaching 95 %, even at the end of the fourth cycle. This result undoubtedly demonstrates that PPy_{DCM} photocatalysts remain very stable with cycling. The small decrease in degradation rate should not be attributed to a reduction of photocatalytic efficiency of PPy_{DCM} material. On the contrary, it should be explained by the decrease in the amount of PPy_{DCM} material (loss of mass) due to the repeated centrifugation and washing steps at the end of each photocatalytic cycle. Note that similar results were also obtained with PPy_{H2O} materials highlighting their stability upon cycling. Remarkably, the high photocatalytic activity of PPy_{DCM} combined with its stability give a glimpse of very promising applications by using

such a radiosynthesized material in water treatment and more generally in alternative photocatalytic treatments.

The mechanism of photocatalytic process involving conducting polymers as photocatalysts was studied in previous works (with addition of radical scavengers) and discussed in detail (Floresyona et al., 2017; Ghosh et al., 2015a; Yuan et al., 2019). In these studies, conjugated polymers always behave as organic semiconductors. When a conjugated polymer based photocatalyst is excited with photons whose energy is higher than its optical band gap (E_g), electrons (e^-) and holes (h^+) are generated: electrons are promoted from the valence band (VB) to conduction band (CB), leaving holes (h^+) in the VB as illustrated in **Figure 7**. As a consequence, photons with energies higher than 1.30 eV ($\lambda \leq 954$ nm) generate excess electrons and holes within PPy_{DCM} materials, while photons with much higher energy (≥ 2.31 eV, $\lambda \leq 537$ nm) are required in case of PPy_{H2O}. Due to the lower optical band gap of PPy_{DCM}, less energy is effectively needed to promote an electron to the conduction band and as a result, more electronic transitions are likely to occur at higher wavelength radiations compared to PPy_{H2O}. This evidently explains the superior photocatalytic activity of PPy_{DCM} in particular in the visible part of the solar spectrum. Note that the high UV and visible light absorption of PPy_{DCM}, compared to that of PPy_{H2O} (see **Figure 1**), also explains its enhanced photocatalytic activity.

A high photocatalytic activity is also related to an efficient separation of the photoexcited electron-hole pairs generated within the photocatalysts after their excitation, which is certainly the case for both PPy_{DCM} and PPy_{H2O} materials. When the electrons and holes escape the recombination process, they can indeed migrate and reach the surfaces of PPy_{DCM} and PPy_{H2O} materials and then interact with molecules present in the surrounding medium, namely water molecules and dissolved oxygen, forming in particular hydroxyl ($HO^\bullet$) and superoxide ($O_2^{\bullet-}$) radicals (Floresyona et al., 2017; Kumar et al., 2020; Yuan et al., 2019)**.** These reactive species finally act as oxidizing species towards organic pollutants leading to their subsequent photodegradation and mineralization as demonstrated in previous works (Ghosh et al., 2015a, 2015b; Floresyona et al., 2017; Yuan et al., 2019) and as summarized in **Figure 7** in the case of photocatalytic degradation of phenol by both PPy_{DCM} and PPy_{H2O} under UV and visible light.

4. Conclusion

In the present work, in the absence of any template and without using any external dopant, two kinds of conducting polymers were radiolytically prepared at an irradiation dose of 72 kGy

directly in the bulk of a solution: PPy_{H2O} material was synthesized in water, while PPy_{DCM} was obtained in DCM solvent. Both polymers were found amorphous and appeared as nanostructured materials with similar morphologies. Nevertheless, contrarily to PPy_{H2O} polymers which were found overoxidized, PPy_{DCM} materials were produced in a doping state and characterized by a very low optical band gap and an intense absorption in the UV, the visible and the near-infrared spectral regions.

Radiolytically produced PPy_{H2O} and PPy_{DCM} materials were then used as photocatalysts for degradation of phenol under either UV or visible light irradiation. Both materials were found stable upon cycling, easily removable from the liquid phase without appreciable loss of activity and thus as a consequence industrially reusable. Moreover, the photocatalytic activity of PPy_{DCM} was shown to be remarkably high and much greater than that of PPy_{H2O}. Notably, the superior activity of PPy_{DCM} was found higher than that of most of the best conducting polymer based photocatalysts, namely PDPB, PPy and P3HT nanostructures, which were previously prepared in hexagonal mesophases by the way of chemical or photochemical polymerizations. The very promising photocatalytic properties of PPy_{DCM} were logically explained by their doping state, their very low optical band gap and their large extended absorption band from the UV to the near infrared region.

The present work definitely provides a facile way to develop cheap and very active metal-free photocatalysts. Indeed, it validates radiation chemistry as a simple method to prepare, within the bulk of a solution, efficient conducting polymer based photocatalysts. However, even if radiolytically synthesized PPy_{DCM} material is triggering hopes for its use as photocatalyst in different environmental applications, its photocatalytic activity still remains slightly lower than that of PEDOT nanospindles which were previously prepared by chemical polymerization within soft templates. This encourages us to adjust the conditions of radiolytic synthesis of PPy (solvent, absorbed dose, dose rate…) in order to optimize their physichochemical properties (band gap value, absorption properties, doping state, stability, processability) and thus to enhance their photocatalytic activity.

Also, work is in due course in order to evaluate the photocatalytic activity of alternative conducting polymers which we already successfully produced by water and DCM radiolysis: PEDOT, P3HT and PTAA polymers as well as their copolymers (Bahry et al., 2021a, 2021b, 2020, 2018). Particular emphasis will be placed on PEDOT synthesized by DCM radiolysis. Finally, as perspective to this work and for environmental purposes the use of PPy_{DCM} and other radiosynthesized conducting polymers, will be investigated for other applications such as air treatment, self-cleaning surfaces, water splitting, energy conversion and hydrogen production.

Author information

*Corresponding author. E-mail: samy.remita@universite-paris-saclay.fr
Tel.: +33 (0)1 69 15 44 41.

Conflicts of interest

There are no conflicts of interest to declare. The authors declare that they have no known competing financial interests or personal relationships that could have appeared to influence the work reported in this paper.

Acknowledgments

The authors thank the Algerian Ministry of Higher Education and Scientific Research for the financial support of Yamina Chouli via the scholarship “Programme National Exceptionnel”.

References

Abdulla, H.S., Abbo, A.I., 2012. Optical and electrical properties of thin films of polyaniline and polypyrrole. Int. J. Electrochem. Sci. 7, 10666–10678.

Andrade, L.S., Laurindo, E.A., De Oliveira, R. V., Rocha-Filho, R.C., Cass, Q.B., 2006. Development of a HPLC method to follow the degradation of phenol by electrochemical or photoelectrochemical treatment. J. Braz. Chem. Soc. 17, 369-373. https://doi.org/10.1590/S0103-50532006000200022

Bahry, T., Cui, Z., Dazzi, A., Gervais, M., Sollogoub, C., Goubard, F., Bui, T.T., Remita, S., 2021a. Radiation-induced polymerization of 3-hexylthiophene in oxygen-free and oxygen-saturated dichloromethane solvent. Radiat. Phys. Chem. 180, 109291-109302. https://doi.org/10.1016/j.radphyschem.2020.109291

Bahry, T., Cui, Z., Deniset-Besseau, A., Gervais, M., Mbomekalle, I., Sollogoub, C., Aubert, P.H., Bui, T.T., Remita, S., 2020. Optimal strategy based on radiation chemistry for facile and direct synthesis of poly(3-thiophene acetic acid) polymers in water and dichloromethane. New J. Chem. 44, 11652-11666. https://doi.org/10.1039/d0nj01474e

Bahry, T., Cui, Z., Deniset-Besseau, A., Gervais, M., Sollogoub, C., Bui, T.T., Remita, S., 2018. An alternative radiolytic route for synthesizing conducting polymers in an organic solvent. New J. Chem. 42, 8704-8716. https://doi.org/10.1039/c8nj01041b

Bahry, T., Khurshid, B., Chouli, Y., Abou Zeid, S., Sollogoub, C., Gervais, M., Bui, T.T., Goubard, F., Remita, S., 2021b. Gamma rays as an innovative tool for synthesizing conducting copolymers with improved properties. New J. Chem. 45, 13142-13157. https://doi.org/10.1039/d1nj02300d

Basavarajappa, P.S., Patil, S.B., Ganganagappa, N., Reddy, K.R., Raghu, A. V., Reddy, C.V., 2020. Recent progress in metal-doped TiO2, non-metal doped/codoped TiO2 and TiO2 nanostructured hybrids for enhanced photocatalysis. Int. J. Hydrogen Energy 45, 7764-7778. https://doi.org/10.1016/j.ijhydene.2019.07.241

Chen, X., Yu, N., Zhang, L., Liu, Z., Wang, Z., Chen, Z., 2015. Synthesis of polypyrrole nanoparticles for constructing full-polymer UV/NIR-shielding film. RSC Adv. 5, 96888-96895. https://doi.org/10.1039/c5ra20164k

Chougule, M., Sen, S., Patil, V., 2012. Facile and efficient route for preparation of polypyrrole-

ZnO nanocomposites: Microstructural, optical, and charge transport properties. J. Appl. Polym. Sci. 125, E541-E547.

Chougule, M.A., Pawar, S.G., Godse, P.R., Mulik, R.N., Sen, S., Patil, V.B., 2011. Synthesis and Characterization of Polypyrrole (PPy) Thin Films. Soft Nanosci. Lett. 01, 6-10. https://doi.org/10.4236/snl.2011.11002

Cristina Sertori Paschoalino, F., Paes Paschoalino, M., Jordão, E., de Figueiredo Jardim, W., 2012. Evaluation of TiO2, ZnO, CuO and Ga2O3 on the Photocatalytic Degradation of Phenol Using an Annular-Flow Photocatalytic Reactor. Open J. Phys. Chem. 02, 135–140. https://doi.org/10.4236/ojpc.2012.23018

Cui, Z., Coletta, C., Dazzi, A., Lefrancois, P., Gervais, M., Néron, S., Remita, S., 2014. Radiolytic method as a novel approach for the synthesis of nanostructured conducting polypyrrole. Langmuir 30, 14086-14094. https://doi.org/10.1021/la5037844

Feng, M., Lu, W., Zhou, Y., Zhen, R., He, H., Wang, Y., Li, C., 2020. Synthesis of polypyrrole/nitrogen-doped porous carbon matrix composite as the electrode material for supercapacitors. Sci. Rep. 10, 1-12. https://doi.org/10.1038/s41598-020-72392-x

Floresyona, D., Goubard, F., Aubert, P.H., Lampre, I., Mathurin, J., Dazzi, A., Ghosh, S., Beaunier, P., Brisset, F., Remita, S., Ramos, L., Remita, H., 2017. Highly active poly(3-hexylthiophene) nanostructures for photocatalysis under solar light. Appl. Catal. B Environ. 209, 23-32. https://doi.org/10.1016/j.apcatb.2017.02.069

Ge, H., Qi, G., Kang, E.T., Neoh, K.G., 1994. Study of overoxidized polypyrrole using X-ray photoelectron spectroscopy. Polymer (Guildf). 35, 504-508. https://doi.org/10.1016/0032-3861(94)90503-7

Ge, J., Zhang, Y., Heo, Y.J., Park, S.J., 2019. Advanced design and synthesis of composite photocatalysts for the remediation of wastewater: A review. Catalysts, 9(2), 122-154. https://doi.org/10.3390/catal9020122

Ghobadi, N., 2013. Band gap determination using absorption spectrum fitting procedure. Int. Nano Lett. 3, 1-4. https://doi.org/10.1186/2228-5326-3-2

Ghosh, S., Kouamé, N.A., Ramos, L., Remita, S., Dazzi, A., Deniset-Besseau, A., Beaunier, P., Goubard, F., Aubert, P.H., Remita, H., 2015a. Conducting polymer nanostructures for photocatalysis under visible light. Nat. Mater. 14, 505-511.

https://doi.org/10.1038/nmat4220

Ghosh, S., Kouame, N.A., Remita, S., Ramos, L., Goubard, F., Aubert, P.H., Dazzi, A., Deniset-Besseau, A., Remita, H., 2015b. Visible-light active conducting polymer nanostructures with superior photocatalytic activity. Sci. Rep. 5, 18002-18011. https://doi.org/10.1038/srep18002

Ghosh, S., Remita, H., Basu R. N., 2017. Conducting Polymers Nanostructures as Novel Materials for Efficient Solar Light Harvesting, Visible light active Photocatalysis. Ghosh, S. (Ed.) in Wiley (2017), p 227-252.

Gürbüz, O., Şenkal, B.F., İçelli, O., 2017. Structural, optical and electrical properties of polypyrrole in an ionic liquid. Polym. Bull. 74, 2625-2639. https://doi.org/10.1007/s00289-016-1856-3

Karim, M.R., Lee, C.J., Lee, M.S., 2007. Synthesis of conducting polypyrrole by radiolysis polymerization method. Polym. Adv. Technol. 18, 916-920. https://doi.org/10.1002/pat.931

Kato, H., Nishikawa, O., Matsui, T., Honma, S., Kokado, H., 1991. Fourier transform infrared spectroscopy study of conducting polymer polypyrrole: Higher order structure of electrochemically synthesized film. J. Phys. Chem. 95, 6014-6016. https://doi.org/10.1021/j100168a055

Kowalska, E., Mahaney, O. O. P., Abe, R., Ohtani, B, 2010. Visible-Light-Induced Photocatalysis through Surface Plasmon Excitation of Gold on Titania Surfaces. Phys. Chem. Chem. Phys. 12, 2344-2355.

Kumar, R., Travas-Sejdic, J., Padhye, L.P., 2020. Conducting polymers-based photocatalysis for treatment of organic contaminants in water. Chem. Eng. J. Adv. 4, 100047-100055. https://doi.org/10.1016/j.ceja.2020.100047

Lei, J., Martin, C.R., 1992. Infrared investigations of pristine polypyrrole - Is the polymer called polypyrrole really poly(pyrrole-co-hydroxypyrrole)? Synth. Met. 48, 331-336. https://doi.org/10.1016/0379-6779(92)90236-C

Li, X.G., Li, A., Huang, M.R., Liao, Y., Lu, Y.G., 2010. Efficient and scalable synthesis of pure polypyrrole nanoparticles applicable for advanced nanocomposites and carbon nanoparticles. J. Phys. Chem. C 114, 19244-19255. https://doi.org/10.1021/jp107435b

Liu, S., Chen, X., 2008. A visible light response TiO2 photocatalyst realized by cationic S-doping and its application for phenol degradation. J. Hazard. Mater. 152, 48-55. https://doi.org/10.1016/j.jhazmat.2007.06.062

Malitesta, C., Losito, I., Sabbatini, L., Zambonin, P.G., 1995. New findings on polypyrrole chemical structure by XPS coupled to chemical derivatization labelling. J. Electron Spectros. Relat. Phenomena 76, 629-634. https://doi.org/10.1016/0368-2048(95)02438-7

Mathys, G.I., Truong, V.T., 1997. Spectroscopic study of thermo-oxidative degradation of polypyrrole powder by FT-IR. Synth. Met. 89, 103-109. https://doi.org/10.1016/s0379-6779(98)80122-7

Méndez-Medrano, M.G., Kowalska, E., Lehoux, A., Herissan, A., Ohtani, B., Bahena, D., Briois, V., Colbeau-Justin, C., Rodríguez-López, J., Remita, H. 2016a. Surface modification of TiO_2 with Ag nanoparticles and CuO nanoclusters for application in photocatalysis. J. Phys. Chem. C, 120, 5143-5154. https://doi.org/10.1021/acs.jpcc.5b10703.

Méndez-Medrano, M.G., Kowalska, E., Lehoux, A., Herissan, A., Ohtani, B., Rau, S., Colbeau-Justin, C., Rodríguez-López, J.L., Remita, H. 2016b. Surface Modification of TiO_2 with Au Nanoclusters for Efficient Water Treatment and Hydrogen Generation under Visible Light. J. Phys. Chem. C. 120 (43), 25010–25022. https://doi.org/10.1021/acs.jpcc.6b06854

Mesa, J.J.M., Arias, J.A.G., Rojas, H.A., Espinosa, O.E.C., 2020. Photocatalytic degradation of Phenol, Catechol and Hydroquinone over Au-ZnO nanomaterials. Rev. Fac. Ing. 94, 24-32. https://doi.org/10.17533/udea.redin.20190513

Ohtani, B., Mahaney, O.O.P., Amano, F., Murakami, N., Abe, R., 2010. What are titania photocatalysts? An exploratory correlation of photocatalytic activity with structural and physical properties, Journal of Advanced Oxidation Technologies, 13, 247-261. https://doi.org/10.1515/jaots-2010-0303.

Patel, J., Yuan, X., Mendes Marinho, S., Leibl, W., Remita, H., Aukauloo; A., 2020. Visible Light-Driven Simultaneous Water Oxidation and Quinone Reduction by Nano-Structured Conjugated Polymer Without Co-catalysts. *Chem. Sci.* 11, 7324-7328. https://doi.org/10.1039/d0sc02122a

Pfluger, P., Street, G.B., 1984. Chemical, electronic, and structural properties of conducting

heterocyclic polymers: A view by XPS. J. Chem. Phys. 80, 544-553. https://doi.org/10.1063/1.446428

Rezaul Karim, M., Lee, C.J., Sarwaruddin Chowdhury, A.M., Nahar, N., Lee, M.S., 2007. Radiolytic synthesis of conducting polypyrrole/carbon nanotube composites. Mater. Lett. 61, 1688-1692. https://doi.org/10.1016/j.matlet.2006.07.100

Sánchez-Rodríguez, D., Méndez Medrano, M.G., Remita, H., Escobar-Barrios, V., 2018. Photocatalytic properties of BiOCl-TiO_2 composites for phenol photodegradation. J. Env. Chem. Eng. 6, 1601–1612

Šetka, M., Calavia, R., Vojkůvka, L., Llobet, E., Drbohlavová, J., Vallejos, S., 2019. Raman and XPS studies of ammonia sensitive polypyrrole nanorods and nanoparticles. Sci. Rep. 9, 8465-8474. https://doi.org/10.1038/s41598-019-44900-1

Setka, M., Raul, C., Vojkuvka, L., Polcak, J., Llobet, E., Drbohlavova, J., Vallejos, S., 2020. Electrochemically deposited polypyrrole nanorods and study of their ammonia sensing properties, in: Materials Today: Proceedings, 20(3), 305-310. https://doi.org/10.1016/j.matpr.2019.10.067

Stejskal, J., 2020. Interaction of conducting polymers, polyaniline and polypyrrole, with organic dyes: polymer morphology control, dye adsorption and photocatalytic decomposition. Chem. Pap. 74, 1-54. https://doi.org/10.1007/s11696-019-00982-9

Tabačiarová, J., Mičušík, M., Fedorko, P., Omastová, M., 2015. Study of polypyrrole aging by XPS, FTIR and conductivity measurements. Polym. Degrad. Stab. 120, 392-401. https://doi.org/10.1016/j.polymdegradstab.2015.07.021

Tauc, J., Menth, A., 1972. States in the gap. J. Non. Cryst. Solids 8–10, 569-585. https://doi.org/10.1016/0022-3093(72)90194-9

Upadhyay, G.K., Rajput, J.K., Pathak, T.K., Kumar, V., Purohit, L.P., 2019. Synthesis of ZnO:TiO2 nanocomposites for photocatalyst application in visible light. Vacuum 160, 154-163. https://doi.org/10.1016/j.vacuum.2018.11.026

Vetter, C.A., Suryawanshi, A., Lamb, J.R., Law, B., Gelling, V.J., 2011. Novel synthesis of stable polypyrrole nanospheres using ozone. Langmuir 27, 13719-13728. https://doi.org/10.1021/la202947e

Warren, M.R., Madden, J.D., 2006. A structural, electronic and electrochemical study of

polypyrrole as a function of oxidation state. Synth. Met. 156, 724-730. https://doi.org/10.1016/j.synthmet.2006.04.004

Wynne, K.J., Street, G.B., 1985. Poly(pyrrol-2-ylium tosylate): Electrochemical Synthesis and Physical and Mechanical Properties. Macromolecules 18, 2361-2368. https://doi.org/10.1021/ma00154a005

Xu, J. , Ao, Y., Chen, M., Fu, D., 2010. Photoelectrochemical property and photocatalytic activity of N-doped TiO_2 nanotube arrays. Appl. Surf. Sci. 256, 4397–4401. http://dx.doi.org/10.1016/j.apsusc.2010.02.037.

Yuan, X., Dragoe, D., Beaunier, P., Uribe, D.B., Ramos, L., Méndez-Medrano, M.G., Remita, H., 2020. Polypyrrole nanostructures modified with mono- And bimetallic nanoparticles for photocatalytic H2 generation. J. Mater. Chem. A 8, 268–277. https://doi.org/10.1039/c9ta11088g

Yuan, X., Floresyona, D., Aubert, P.H., Bui, T.T., Remita, S., Ghosh, S., Brisset, F., Goubard, F., Remita, H., 2019. Photocatalytic degradation of organic pollutant with polypyrrole nanostructures under UV and visible light. Appl. Catal. B Environ. 242, 284-292. https://doi.org/10.1016/j.apcatb.2018.10.002

Yuan, X., Wang, C., Dragoe, D., Beaunier, P., Colbeau-Justin, C., Remita, H., 2021. Highly Promoted Photocatalytic Hydrogen Generation by Multiple Electron Transfer Pathways. Appl. Catal. B Environ. 281, 119457-119465. https://doi.org/10.1016/j.apcatb.2020.119457

Scheme 1

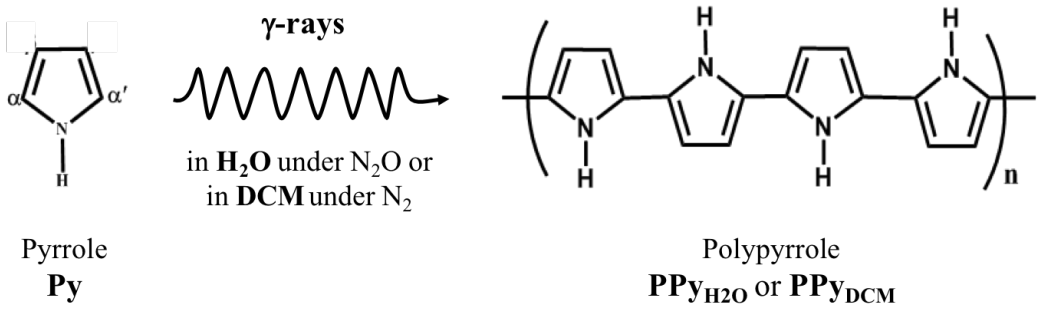

Scheme 1- *Radiation-induced polymerization of Pyrrole (Py) monomers in water under N_2O or in dichloromethane (DCM) under N_2, leading respectively to PPy_{H2O} and PPy_{DCM} polymers.*

Figure 1

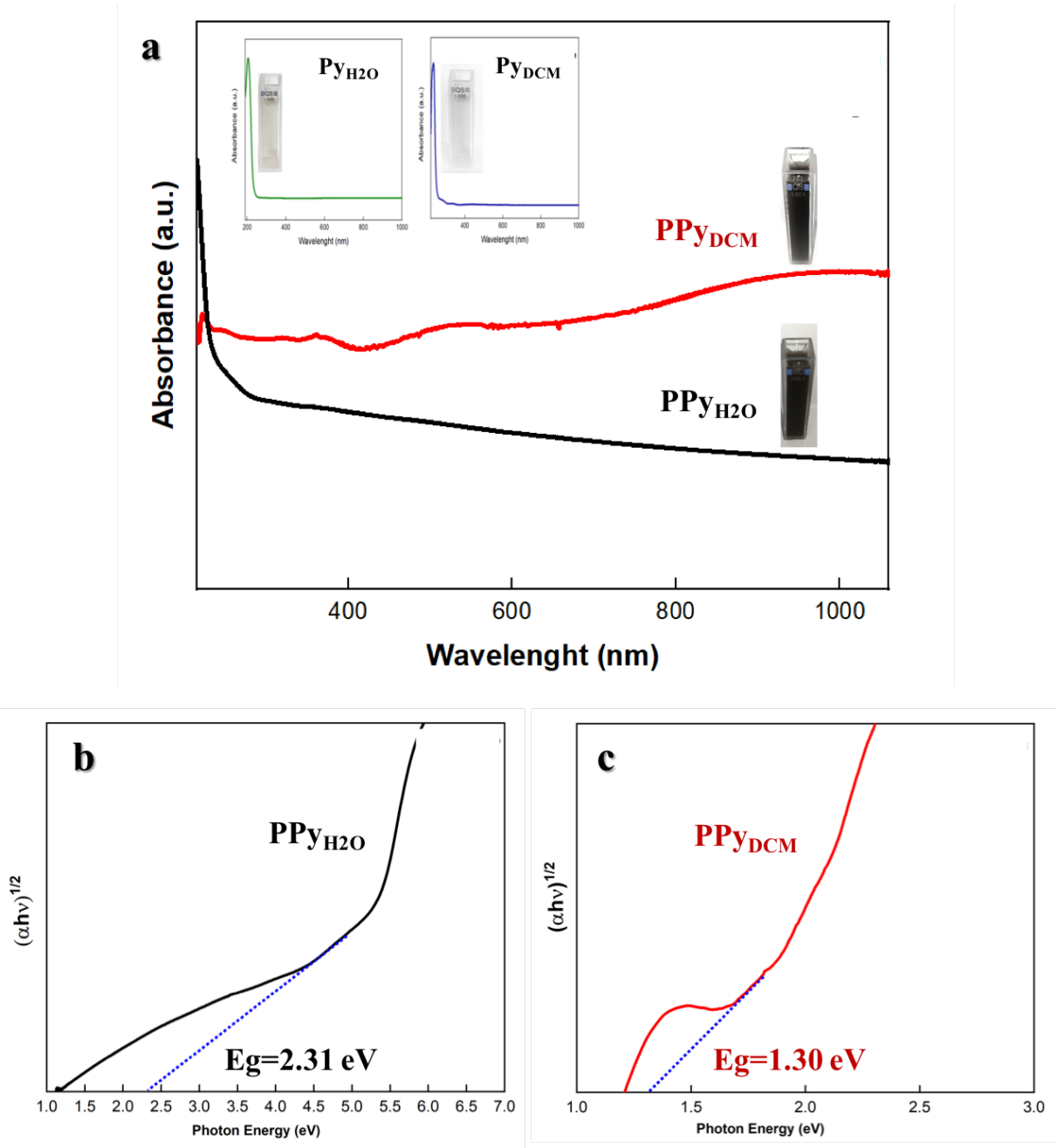

Figure 1- a) *UV-Vis absorption spectra and photographs of PPy$_{H2O}$ and PPy$_{DCM}$ aqueous and DCM solutions obtained after γ-irradiation at 72 kGy.* **Inset)** *UV-Vis absorption spectra and photographs of pyrrole aqueous (Py$_{H2O}$) and DCM (Py$_{DCM}$) solutions. Initial concentration of Py monomers was 20 mM and references were pure solvents in all cases.* **b) and c)** *Tauc's plot analysis of UV-Vis absorption spectra of PPy$_{H2O}$ and PPy$_{DCM}$ for optical band gap assessment.*

Figure 2

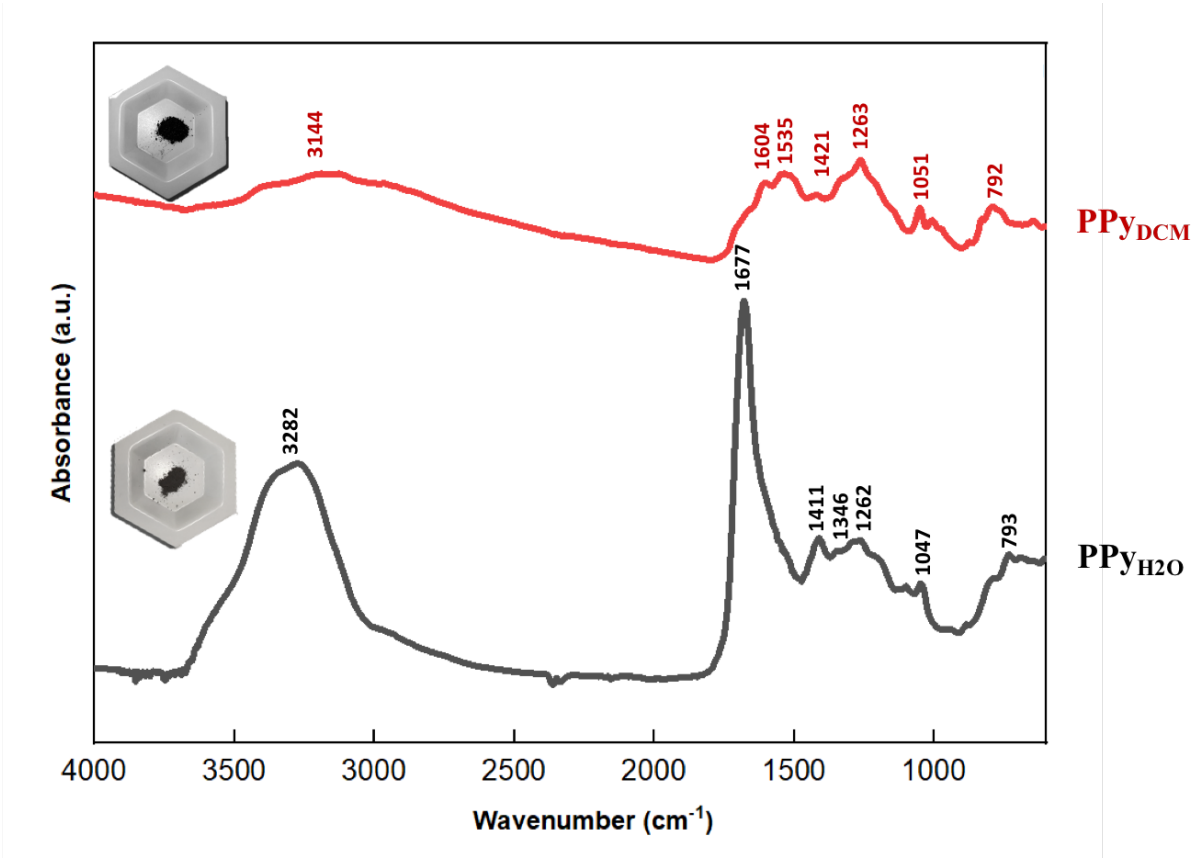

Figure 2- *ATR-FTIR spectra and photographs of PPy_{H2O} and PPy_{DCM} polymer powders obtained after γ-irradiation at 72 kGy of an aqueous solution under N_2O or a DCM solution under N_2 atmosphere. Initial concentration of Py monomers was 20 mM in both cases.*

Figure 3

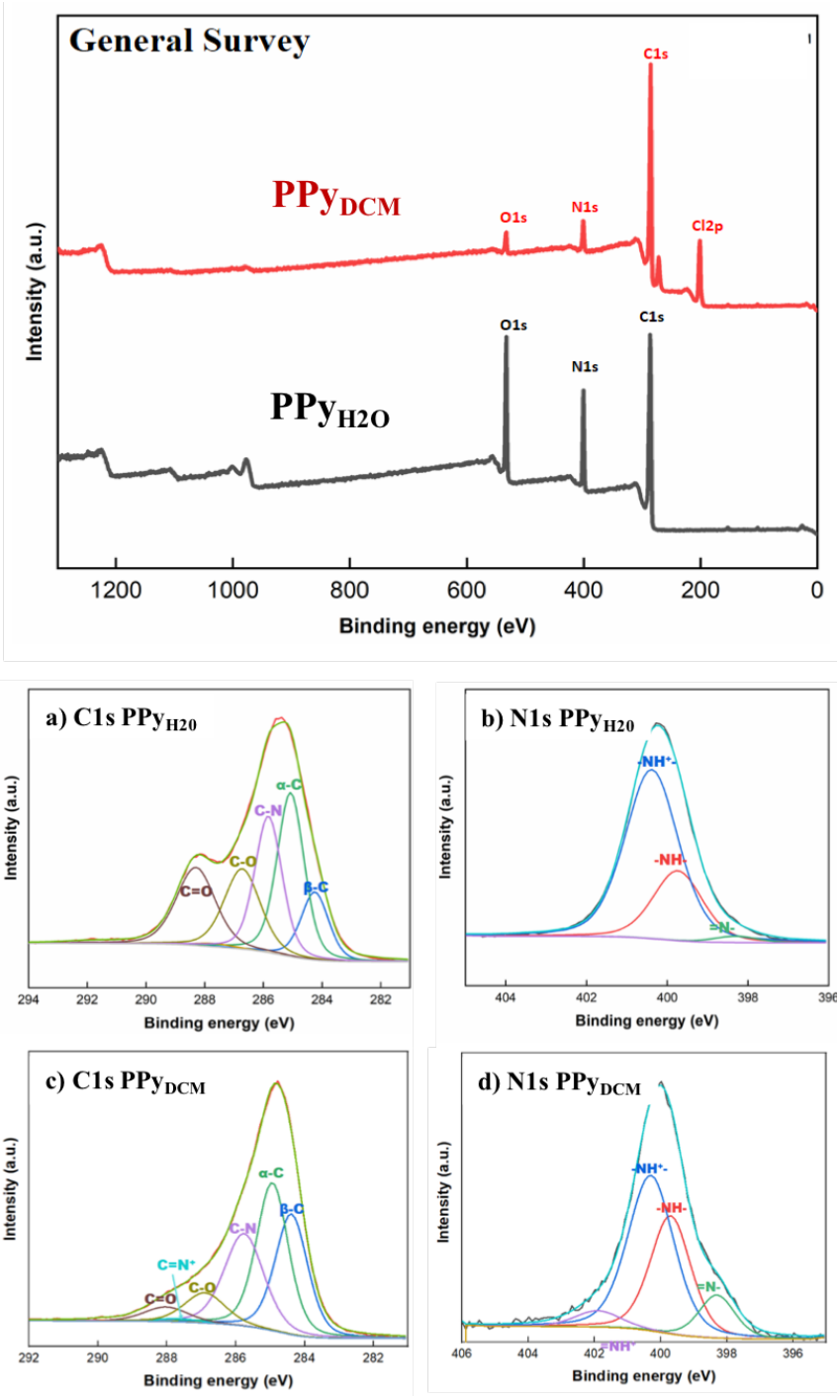

Figure 3- *XPS General Survey spectra of PPy_{H2O} and PPy_{DCM} polymers obtained after γ-irradiation at 72 kGy of an aqueous solution under N_2O or a DCM solution under N_2 atmosphere. Initial concentration of Py monomers was 20 mM in both cases. High C1s and N1s resolution spectra with deconvoluted peaks from PPy_{H2O} and PPy_{DCM}:* **a)** *C1s from PPy_{H2O},* **b)** *N1s from PPy_{H2O},* **c)** *C1s from PPy_{DCM} and* **d)** *N1s from PPy_{DCM}.*

Figure 4

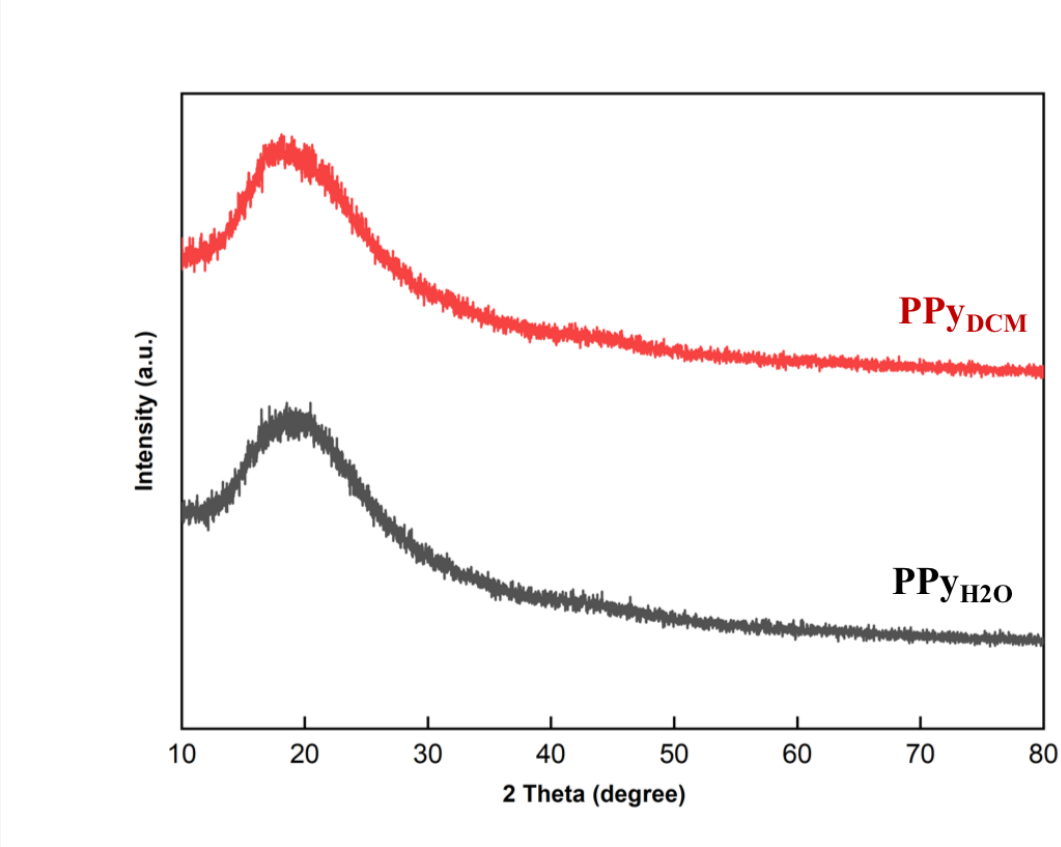

Figure 4- *XRD patterns of PPy_{H2O} and PPy_{DCM} polymer powders obtained after γ-irradiation at 72 kGy of an aqueous solution under N_2O or a DCM solution under N_2 atmosphere. Initial concentration of Py monomers was 20 mM in both solutions. The substrate used for XRD analysis was aluminium.*

Figure 5

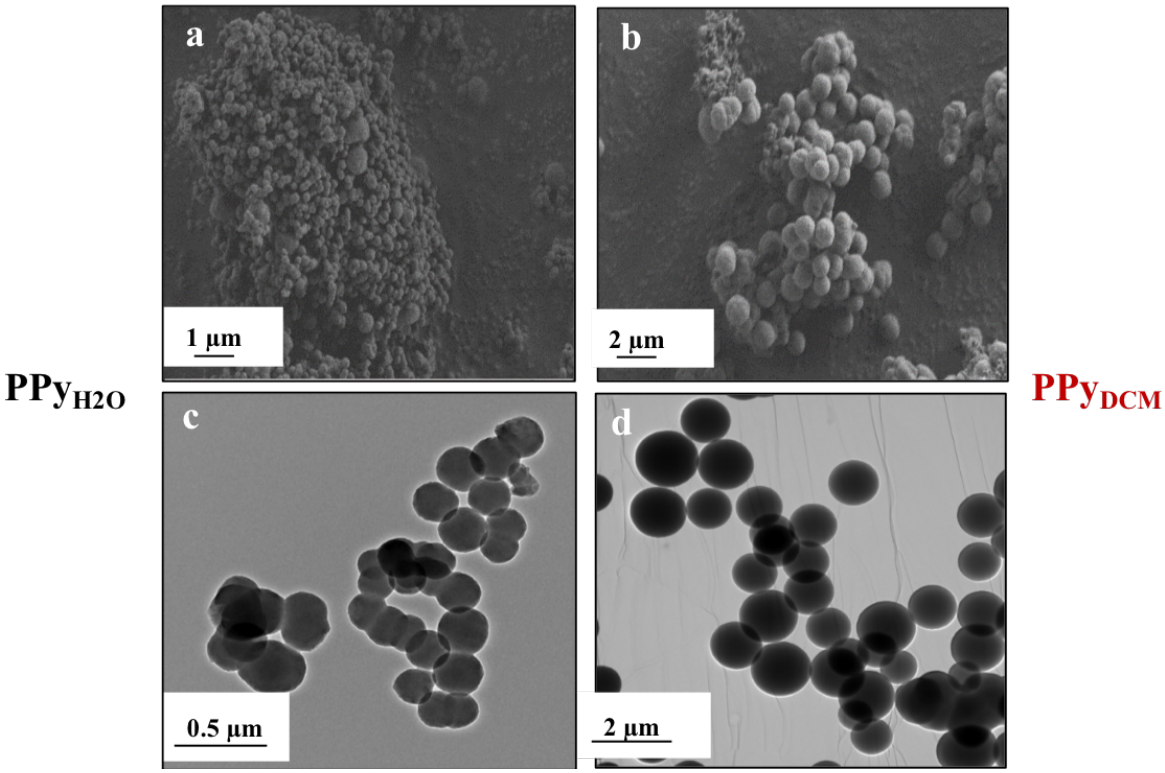

Figure 5- *Morphological characterizations of radiosynthesized PPy polymers: SEM images of* **a)** *PPy_{H2O} and* ***b)*** *PPy_{DCM} polymers as well as TEM images of* ***c)*** *PPy_{H2O} and* ***d)*** *PPy_{DCM} polymers. PPy polymers were obtained after γ-irradiation at 72 kGy of an aqueous solution under N_2O or a DCM solution under N_2 atmosphere. Initial concentration of Py monomers was 20 mM in all cases.*

Figure 6

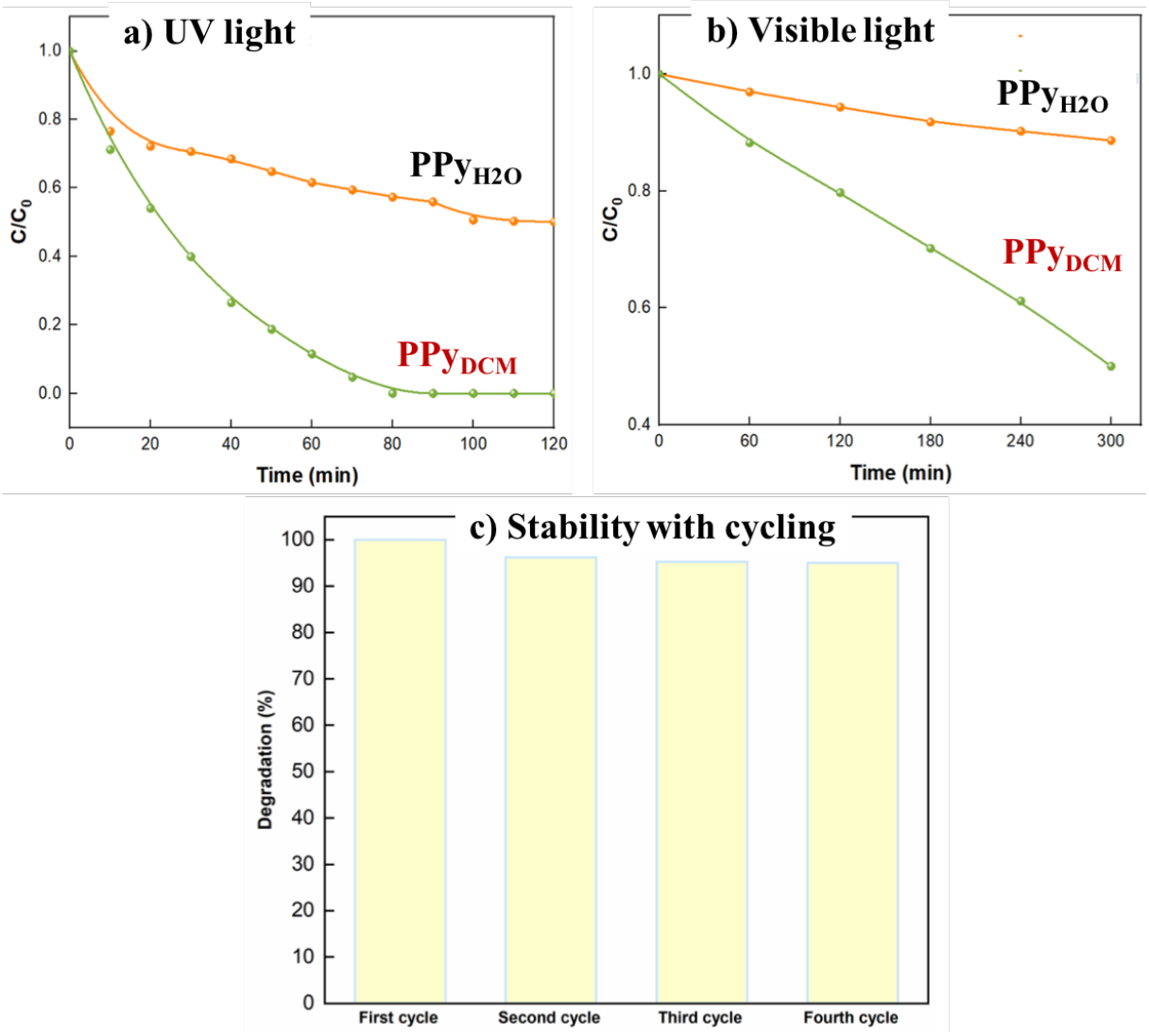

Figure 6- *Photocatalytic degradation rate of phenol using PPy_{H2O} and PPy_{DCM} under* ***a)*** *UV light and* ***b)*** *Visible light.* ***c)*** *Evaluation of the reusability of PPy_{DCM} photocatalysts with cycling. PPy polymers were obtained after γ-irradiation at 72 kGy of an aqueous solution under N_2O or a DCM solution under N_2 atmosphere. Initial concentration of Py monomers was 20 mM in all cases.*

Figure 7

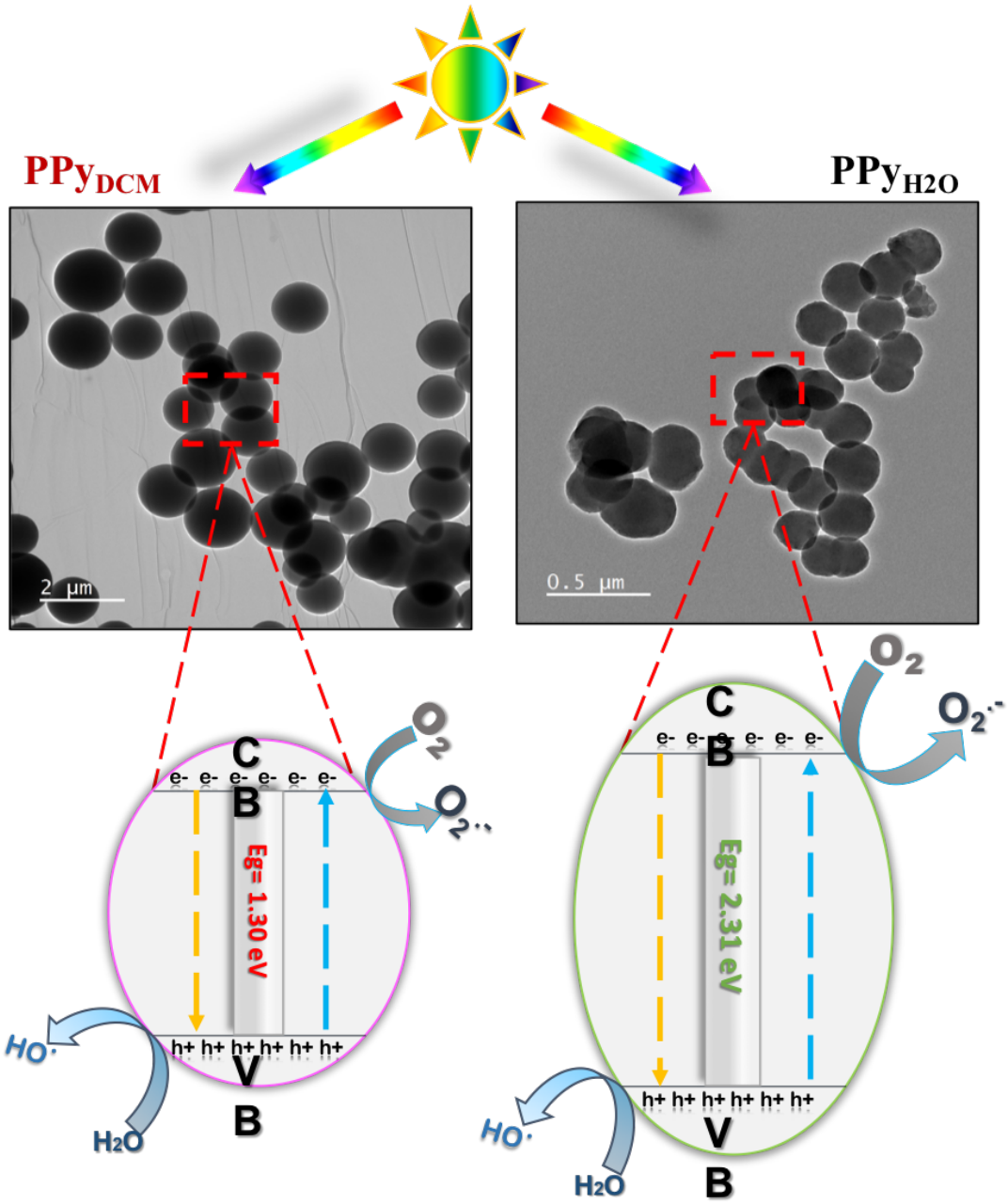

Figure 7- *Proposed mechanism of photocatalytic degradation of phenol by* PPy_{H2O} *and* PPy_{DCM} *under UV and Visible light irradiation.*

Graphical abstract

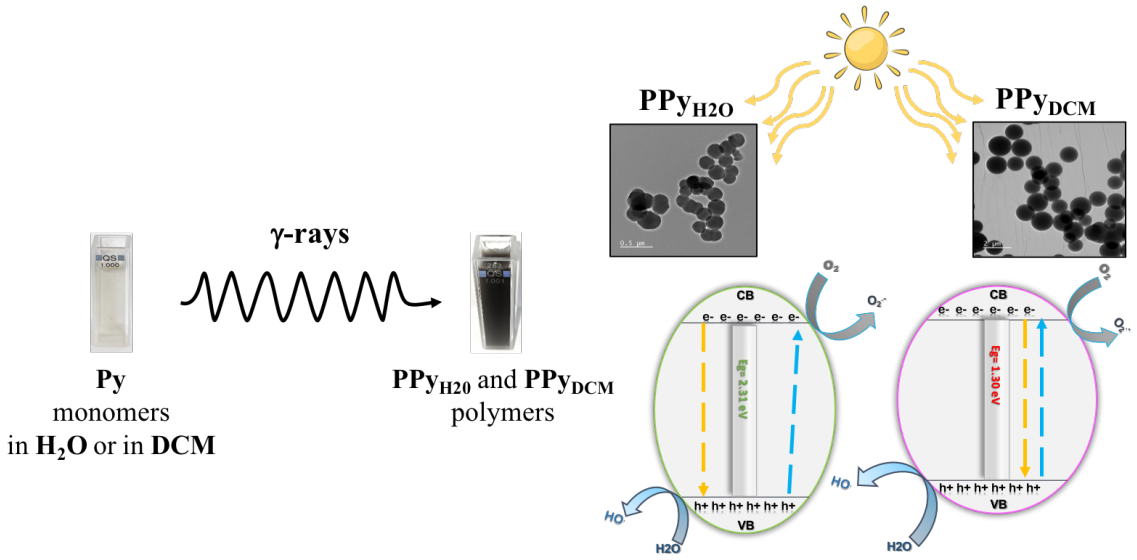

Highlights

Radiolysis is used for the synthesis of PPy_{H2O} and PPy_{DCM} polymers in water and DCM.

PPy_{DCM} is produced in a doping state with a very low band gap and an intense absorption.

PPy_{H2O} and PPy_{DCM} are used as photocatalysts for phenol degradation under UV and Vis light.

Photocatalytic activity of PPy_{DCM} is remarkably high and much greater than that of PPy_{H2O}.

PPy_{DCM} is found as one of the best conducting polymers based photocatalysts.